Magnetic Resonance in Medicine 51:533–541 (2004)

In Vivo Assessment of Tumoral Angiogenesis

I. Troprès,[1*] L. Lamalle,[1] M. Péoc'h,[1] R. Farion,[1] Y. Usson,[2] M. Décorps,[1] and C. Rémy[1]

Vessel size imaging (VSI) for brain tumor characterization was evaluated and the vessel size index measured by MRI (VSI_{MRI}) was correlated with VSI obtained by histology (VSI_{histo}). Blood volume (BV) and VSI maps were obtained on 12 rats by simultaneous measurements of R_2* and R_2, before and after the injection of a macromolecular contrast agent, AMI-227. Immunostaining of collagen IV in vessels was performed. An expression was derived for evaluating VSI from stereologic measurements on histology data (VSI_{histo}). On BV and VSI images obtained from large-size tumors (n = 9), three regions could be distinguished and correlated well with histological sections: a high BV region surrounding the tumor, a necrotic area where BV is very low, and a viable tumor tissue region showing lower BV but higher VSI than the normal rat cortex, with the presence of larger vessels. The quantitative analysis showed a good correlation (Spearman rank's rho = 0.74) between VSI_{histo} and VSI_{MRI} with a linear regression coefficient of 1.17. The good correlation coefficient supports VSI imaging as a quantitative method for tumor vasculature characterization. Magn Reson Med 51: 533–541, 2004. © 2004 Wiley-Liss, Inc.

Key words: vessel size index imaging; rats; gliomas; USPIO

Angiogenesis is an important stage in tumor development. Neovascularization, which is associated with rapid tumor growth, is characterized by a higher vessel density in some areas of the tumor and by vessels of larger lumen than in normal tissues (1). Microvessel density was found to be a major factor in predicting the aggressiveness of the disease (2) and patient survival in different tumor types (2–5). This is currently determined by immunohistochemistry on biopsies. Nevertheless, regional tumor heterogeneity limits the use of this technique for routine examinations since biopsy samples are small and might not be sampled in the most aggressive or representative part of the tumor. In addition, its invasiveness prevents the use of this technique for therapy follow-up.

Among the possible imaging methods for vascularization characterization, perfusion MR techniques allow brain microvascularization assessment, are noninvasive, and provide a high spatial resolution. Blood volume (BV) imaging could be a noninvasive alternative to histology since an increase in the mean vessel density and/or vessel lumen can be detected through an increase in BV. For example, in rat mammary adenocarcinoma models, statistically significant differences were observed by Okuhata et al. (6) in MRI-estimated tumor BV between tumor subtypes and between the tumor periphery and tumor center. More recently, Dennie et al. (7) suggested that the ratio of gradient-echo and spin-echo relaxation rate changes ($\Delta R_2^*/\Delta R_2$) induced by a high molecular weight contrast agent provides an indication of the average vessel size in a voxel, under certain conditions related to the echo time, the contrast agent concentration, and the main magnetic field (8). A good correspondence between MRI and histology results was shown in a rat glioma model (7). More recently, the $\Delta R_2^*/\Delta R_2$ ratio obtained after Gd-DTPA injection was found to correlate strongly with tumor grade (9) in patients with brain tumors. However, access to the morphology of the vessels is not straightforward, since correlation with histology necessitates Monte-Carlo simulations (7). $\Delta R_2^*/\Delta R_2$ is a dimensionless ratio and its expression in terms of tissue model parameters depends, in addition to the vessel size distribution, on the contrast agent concentration and the water diffusion coefficient, as discussed by Jensen and Chandra (eq. 24 of Ref. 10). To avoid strong dependency on contrast agent concentration, these authors rather suggest the use of a quantity Q, defined as the ratio $\Delta R_2/(\Delta R_2^*)^{2/3}$ and expressed in $s^{-1/3}$, which was shown to depend only on intrinsic tissue properties such as the BV fraction, the vessel size distribution and the tissue water diffusion coefficient (eq. 23 of Ref. 10). The underlying theory assumes appropriate choice of contrast agent concentration and echo times (eqs. 12, 13, 21, 22 of Ref. 10) and supposes small blood volume fractions ($BV \ll 1$). The data of Dennie et al. (7) which satisfy these conditions were used to estimate Q from histology and MRI measurements, with good agreement found by the authors (10). In parallel, we have developed a novel method for vessel size imaging (11) in which a vessel size index (VSI), expressed in micrometers, was defined from the distribution of the vessel sizes only. This index can be easily estimated by MRI from the ratio $(\Delta R_2^*/\Delta R_2)^{3/2}$, the water diffusion coefficient, and the contrast agent concentration. Unlike previous methods, a multipoint technique was used for ΔR_2^* measurements to avoid TE-dependent errors (see discussion in Ref. 11). BV is simultaneously obtained from VSI MRI experiments and both pieces of information, BV and VSI, might become prognostic indicators for tumor angiogenesis (12).

The aim of this work was twofold: to assess the interest of VSI imaging for noninvasive characterization of brain tumor microvasculature, and to further validate the method by comparing the VSI obtained by MRI (VSI_{MRI}) with results from quantitative immunohistology (VSI_{histo}) on the same animals.

[1]Unité mixte INSERM 594/Université Joseph Fourier, Laboratoire de Recherche Conventionné du CEA No. 30V, Hôpital Albert Michallon, and European Synchrotron Radiation Facility, Grenoble, France.

[2]Équipe CNRS UMR5525, Institut Albert Bonniot, Grenoble, France.

Grant sponsors: Association pour la Recherche sur le Cancer, Comité de l'Isère de la Ligue contre le Cancer, programme interdisciplinaire CNRS-INSERM-CEA "Imagerie du petit animal."

Present address for I. Troprès and L. Lamalle: Unité IRM 3T, Hôpital Albert Michallon, Grenoble, France.

*Correspondence to: Irène Troprès, Unité IRM 3T, Hôpital Albert Michallon, 38043 Grenoble Cedex 9, France. E-mail: Irene.Tropres@ujf-grenoble.fr

Received 10 December 2002; revised 17 October 2003; accepted 17 October 2003.

DOI 10.1002/mrm.20017
Published online in Wiley InterScience (www.interscience.wiley.com).

THEORY

The theory underlying the estimation of BV and VSI has been reported previously (11). VSI is the weighted mean, expressed as a distance:

$$VSI = \left[\int_0^\infty r^{-2/3} f(r)\, dr \right]^{-3/2}, \qquad [1]$$

where *f(r)* is defined from $BV \cdot f(r)$, the volume fraction of vessels with radius r and $\int_0^\infty f(r)\, dr = 1$. Briefly, the changes of the relaxation rates R_2* and R_2 induced by the presence of the contrast agent in the blood are measured using, respectively, gradient echo and spin echo imaging sequences, before and after contrast agent injection. Subsequently, VSI can be estimated from the following equation:

$$VSI_{MRI}(\mu m) = 0.424 \left(\frac{D}{\gamma \cdot \Delta\chi \cdot B_0} \right)^{1/2} \left(\frac{\Delta R_2^*}{\Delta R_2} \right)^{3/2}, \qquad [2]$$

where D is the water diffusion coefficient in the tissue ($\mu m^2/s$), $\Delta\chi$ is the increase (induced by the presence of the contrast agent in the vasculature) in the magnetic susceptibility difference 7χ between the extra- and intravascular compartments (nonrationalized cgs emu units), B_0 is the main magnetic field (T), and γ is the gyromagnetic ratio of protons. From NMR measurements, BV is calculated according to the following equation:

$$BV(\%) = \frac{3}{4\pi} \frac{\Delta R_2^*}{\gamma \cdot \Delta\chi \cdot B_0}. \qquad [3]$$

Blood volume is directly obtained from ΔR_2* measurements (gradient echo NMR sequence) and VSI_{MRI} from both ΔR_2 and ΔR_2* measurements (spin echo and gradient echo sequences, respectively), provided the water diffusion coefficient and the susceptibility increase are known. Expressions [2] and [3] are valid for small BV fractions and high blood contrast agent concentrations ($BV \ll 1$, high $\Delta\chi$ (8,11,13)). VSI_{MRI} measurement also necessitates the use of long TEs ($TE \gg 1/(2\pi\gamma\Delta\chi B_0)$ (11,14)) to be independent of the echo time.

VSI can also be calculated from vessel radii measurements on histological sections, leading to an estimated VSI_{histo}. According to Underwood (15), the average areal fraction $\overline{Aa}$, determined on sections through a volume, represents an estimate of BV (Fig. 1). Therefore:

$$BV = \overline{Aa} = \int_0^\infty Aa(r)\, dr, \qquad [4]$$

where *Aa(r)dr* is the areal fraction of vessels with radius *r*. Since $\int_0^\infty f(r)dr = 1$ (Eq. 1), *Aa(r)dr* can be expressed as:

$$Aa(r)\, dr = BV \cdot f(r)\, dr = \overline{Aa} \cdot f(r)\, dr \qquad [5]$$

and therefore:

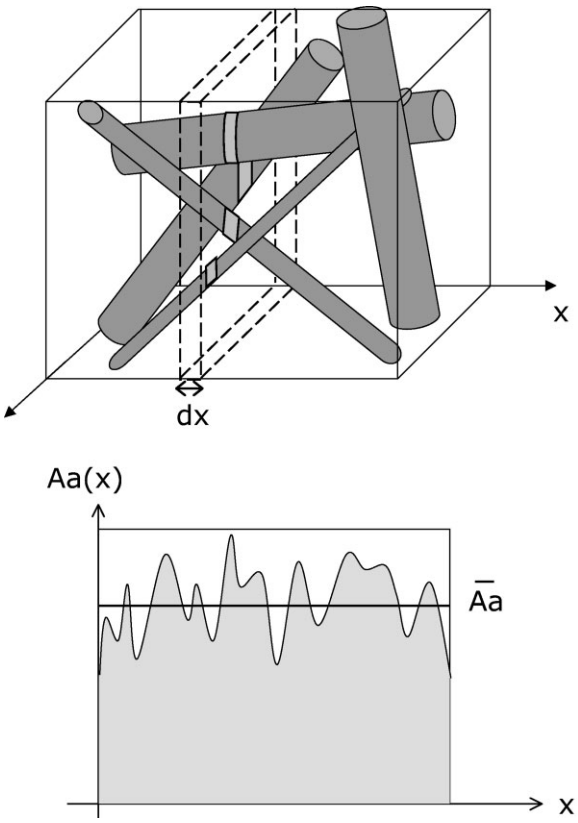

FIG. 1 Estimation of BV by $\overline{Aa}$. Vessels are modeled as cylinders of given radii. The areal fraction of cylinders Aa(x) on sections through a volume is measured and, according to stereology principles (36), its average $\overline{Aa}$ is equal to the blood volume fraction BV occupied by the cylinders in this volume.

$$f(r)\, dr = \frac{Aa(r)\, dr}{\overline{Aa}}. \qquad [6]$$

Using the simple approach of considering vessels as randomly oriented cylinders of a given radius, *Aa(r)* can also be calculated from:

$$Aa(r)\, dr = \frac{2\pi \cdot r^2 \cdot n(r)\, dr}{S}, \qquad [7]$$

where S is the microscope field examined and *n(r)dr* the number of vessels with radius *r*. By substituting Eq. 7 into Eq. 6, the following is obtained:

$$f(r)\, dr = \frac{n(r) \cdot r^2 dr}{\int_0^\infty n(r) \cdot r^2 dr}.$$

Equation 1 then becomes:

$$VSI_{histo} = \left(\frac{\int_0^\infty n(r) \cdot r^{4/3} dr}{\int_0^\infty n(r) \cdot r^2 dr} \right)^{-3/2}$$

or:

$$VSI_{histo} = \left(\frac{\sum_i n(r_i) \cdot r_i^{4/3}}{\sum_i n(r_i) \cdot r_i^2} \right)^{-3/2}, \quad [8]$$

when working with histograms of a constant interval width Δr_i.

MATERIALS AND METHODS

Intracerebral Glioma Model in Rat Brain

Male Wistar rats were anesthetized (400 mg/kg chloral hydrate) and placed on a stereotactic head holder. A scalp incision was performed along the median line. A 2.5-mm diameter burr hole was drilled in the skull 3.5 mm lateral to the bregma. The cell suspension (10^5 cells in 5 μl) was injected in 10 sec using a Hamilton syringe into the right caudate nucleus, at a depth of 3.5 mm under the dura. The syringe was slowly removed 1 min after the injection. The burr hole was plugged with Horsley wax and the scalp sutured. The survival time of the rats was about 4–5 weeks after tumor cell implantation. All procedures related to animal care strictly conformed to the guidelines of the French Government (decree 87-848 of October 19, 1987, licenses 006722 and A38071).

Imaging Protocols

All experiments were performed in a 2.35 T, 40-cm diameter horizontal bore magnet (Bruker Spectrospin, Wissembourg, France), equipped with actively shielded gradient coils (Magnex Scientific, Abingdon, UK) and interfaced to an SMIS console (SMIS, Guildford, UK).

The contrast agent used in this study was a high molecular weight contrast agent, AMI-227 (Sinerem from Guerbet Laboratories, Aulnay-sous-Bois, France) made of ultrasmall superparamagnetic iron oxide (USPIO) particles. Provided that the blood–brain barrier (BBB) is intact, AMI-227 acts like a blood pool contrast agent. Experiments performed on rats bearing a glioma with a similar contrast agent (MION) (7) suggested that, even within the tumor, the contrast agent remained within the vasculature. The half-life in the rat plasma is 120 min for a 30 μmol Fe/kg dose and 4.5 hr for a 200 μmol Fe/kg dose (unpubl. data, Laboratoires Guerbet).

Experiment 1

Within 26–34 days after C6 cell implantation, rats (n = 12) were anesthetized with a mixture of 1.5% halothane in air after induction with 4% halothane. The animal preparation consisted of inserting two 0.7-mm external diameter catheters, one in the femoral vein for i.v. injection of contrast agent, and the other in the femoral artery for mean arterial blood pressure (MABP) measurement and blood sampling for gas analysis. After surgery, halothane was maintained at 0.6%. MABP was measured via a graphic recorder (8000S, Gould Electronics, Balainvilliers, France) and blood gases (PaO_2, $PaCO_2$), blood pH, hematocrit, and oxygen saturation of hemoglobin were analyzed with an ABL510 (Radiometer, Copenhagen, Denmark). Blood samples smaller than 0.1 ml were taken before and immediately after acquisition of each imaging series. The body temperature was monitored by a rectal probe and maintained at 36.8 ± 0.4°C by a heating pad placed under the abdomen.

The rats were placed in the magnet immediately after catheter surgery and preliminary NMR adjustments (tuning, shimming, and acquisition of scout images for positioning) were performed. It was then checked that the physiological parameters were within the normal range. The precontrast images were obtained, in the transverse plane, immediately followed by an injection of AMI-227. After a 3-min delay to allow the contrast agent to distribute homogeneously in the intravascular pool, the postcontrast images were acquired. Three successive injections of AMI-227 were made: the first one of 30 μmol Fe/kg and two others of 100 μmol Fe/kg, resulting in a total injected dose of 230 μmol Fe/kg. Approximately 35 min elapsed between the two injections. The contrast agent dose remaining at the time of the last acquisition can be calculated from the elimination law and the half-life in plasma ($e^{-\lambda t}$ where $\lambda = ln(2)/\tau_{1/2}$; $\tau_{1/2}$ is the contrast agent half-life and t is the elapsed time after injection) and was ~205 μmol Fe/kg. Only images obtained from the last injection were analyzed in the current work. The others were aimed at the study of the effects of contrast agent concentration on VSI evaluation (16).

The imaging sequence consisted of a simultaneous multigradient echo spin echo acquisition described previously (11). Eight contiguous slices were obtained with the nominal image resolution of 0.234 × 0.468 × 1 mm^3 and were zero-filled to 0.468 × 0.468 × 1 mm^3. The number of averages was 2 for a total acquisition time of 12 min. TR was set to 6 sec. The TE values were 9.04, 17.32, 25.60, 33.88, and 42.16 msec for gradient echo images and 100 msec for the spin echo image.

Due to technical problems during the histology process, only four rats were exploitable for the correlation of MRI results with histology. Another experiment was then performed and coronal instead of transverse images were acquired for an easier comparison with histologic sections.

Experiment 2

In the second experiment, three rats were imaged 20–24 days after C6 cells implantation. The rats were anesthetized with a mixture of 30% oxygen, 0.6–1% isoflurane, and air. The animal preparation was the same as described in the first experiment except that MABP was not monitored. Body temperature was maintained at 37.9 ± 1.0°C by a heating pad placed under the abdomen. A single injection of 200 μmol Fe/kg body weight was performed and coronal images were acquired immediately before and 4 min after the injection. The difference between Experiments 1 and 2 lay in the image orientation and in the slice thickness: 1 vs. 1.1 mm.

Immunohistology

At the end of the MRI experiment, intracardiac perfusion was performed under anesthesia. The blood was removed by rinsing with a heparinized saline solution and the brain was fixed by acetic formalin. The brain was then excised,

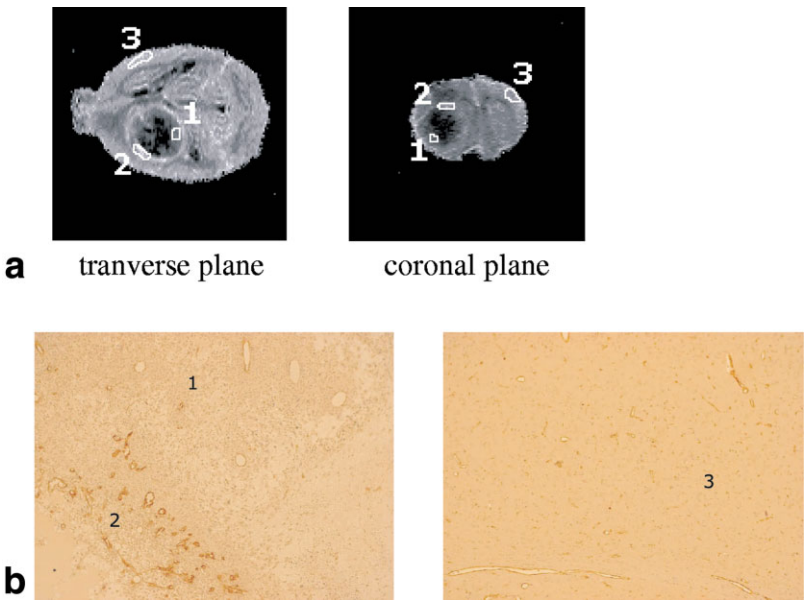

FIG. 2. ROIs drawn on (**a**) the ΔR_2 map of rats from Experiment 1 (transverse plane) and from Experiment 2 (coronal plane) and (**b**) histological sections (×100) corresponding to ROIs on the NMR images. 1 is the intratumoral zone, 2 is the periphery of the tumor, and 3 is the contralateral cortex.

stored in a salted formalin solution, and embedded in paraffin. Two stainings were performed: hematoxylin erythrosin safran (HES) staining was used to characterize brain tumor (localization, size, and tumor regions) and the collagen IV staining procedure resulted in a brown staining of the basement membranes of the blood vessels. Two 5-μm thick sections were analyzed in the corresponding 1-mm thick NMR image.

Slides were analyzed with a SAMBA image analysis system (SAMBA Technologies, France). The image of a 0.27 mm^2 microscope field was collected with an RGB tri-CCD camera (Sony). The blue channel provides the best contrast for the vessel staining and was used for image segmentation and feature extraction. The binary masks of the vessels were obtained by thresholding the gray level histogram of the blue component. A manual correction was sometimes necessary because of the nonhomogenous staining on the slices. The vessel lumina were filled in and a unique label was assigned to each vessel. Then, for all pixels within a vessel, the shortest distance *d* to the edge of

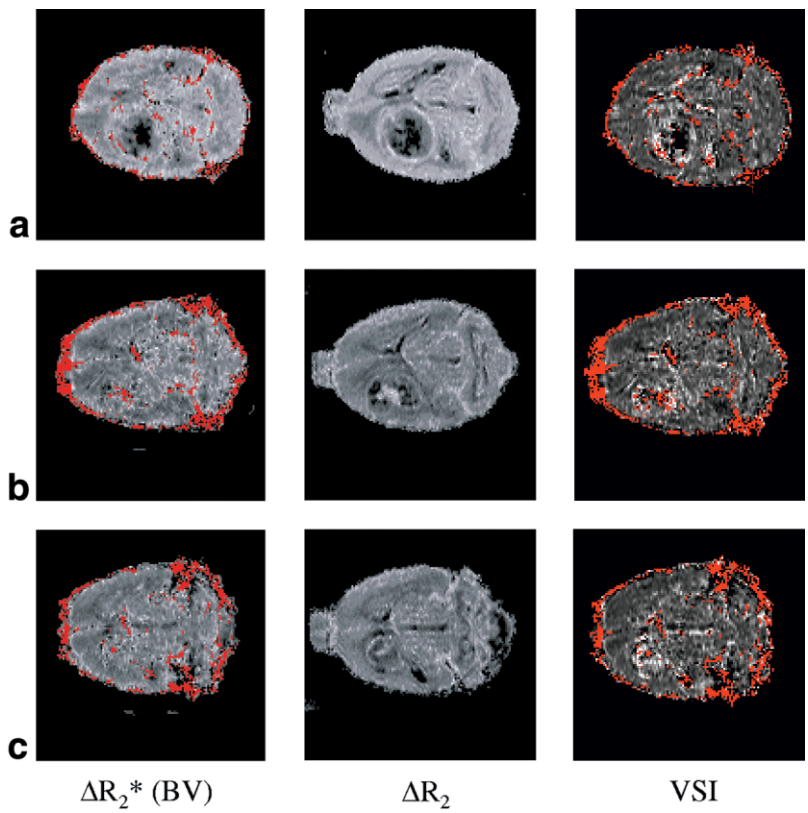

FIG. 3. **a–c:** ΔR_2^*, ΔR_2, and VSI maps of the three different types of tumors: (**a**) large-size tumor, (**b**) medium-size tumor, and (**c**) small size tumor.

the vessel was calculated. The outer radius of each labeled vessel was given by the greatest distance d measured among all pixels in this vessel. Then the vessels were classified according to their diameter and the number, n, of vessels associated with each diameter was reported.

Data Analysis

VSI images were calculated using Eq. [2]. A uniform diffusion coefficient D = 697 $\mu m^2.s^{-1}$ (17) was assumed in the whole brain. The pixels corresponding to a BV exceeding 17% (limit value for the linearity between ΔR_2* and BV) were excluded from the computations (red on the BV and VSI maps). For these pixels, no valid VSI estimation could therefore be performed. The pixels whose value exceeded 100 μm were also colored in red on VSI maps. This threshold was necessary in order to better exploit the gray levels but did not concern in-brain pixels. Whenever ΔR_2* or ΔR_2 was equal to zero due to the absence of the contrast agent, corresponding BV and VSI pixels were set to black (zero). No VSI measurements were made for black or red pixels. Results are expressed as the mean ± standard deviation.

VSI and BV information from NMR acquisitions on six rats from Experiment 1 with a large tumor were analyzed first. Three regions of interest (ROIs) were defined in the contralateral cortex, the periphery of the tumor, and its central part (Fig. 2). They were chosen either on the basis of the SE postinjection image or the ΔR_2 map where normal anatomy and tumor regions could be easily distinguished. The significance of differences between ROIs was tested by the Wilcoxon Signed Rank test ($P < 0.05$) for VSI and BV (StatView SE program, Abacus Concepts, Berkeley, CA).

The second analysis consisted of validation of VSI_{MRI} computations by comparing them to VSI_{histo}. The rats included were chosen according to the quality of the histological sections: n = 4 in Experiment 1 and n = 3 in Experiment 2, corresponding to large and medium-size tumors. For each animal, ROIs were defined on the VSI maps in accordance with the area selected on histological sections (Fig. 2). Red and black pixels were avoided. Since the areas analyzed by histology were very small, only a few pixels were selected. The microscope field in the rim of the tumor was chosen to span the healthy and the tumoral tissue. In the tumor center, the microscope field contained only tumoral tissue. VSI_{histo} was calculated from the mean vessel radius histogram on the two sections. Correlation was evaluated by a Spearman rank correlation test on all data points and the linear regression coefficient (R^2) was calculated zone by zone.

RESULTS

Qualitative Analysis

For Experiments 1 and 2, three types of tumors were observed: nine large-size (diameter > 6 mm) with shifted median line, two medium-size (diameter = 4–5 mm), and four small-size tumors (diameter = 2–3 mm). Ventricles were enlarged in all rats.

For all the animals presented here, the physiological parameters remained within a normal range except for the O_2 saturation for animals in the first experiment (SaO_2 = 88.5% with PaO_2 = 70.5 ± 8.4 mmHg) and a slight hypercapnia for animals in experiment 2 ($PaCO_2$ = 44.8 mmHg, Table 1).

Table 1
Physiological Parameters of All the Animals (Mean ± SD)

	1st experiment n = 12	2nd experiment n = 3
$PaCO_2$ (mm Hg)	35.0 ± 5.0	44.8 ± 2.3
PaO_2 (mm Hg)	70.5 ± 8.4	154.0 ± 21.4
MABP (mm Hg)	108.1 ± 34.2	—
Arterial pH	7.38 ± 0.03	7.37 ± 0.03
Temperature (°C)	36.8 ± 0.4	37.9 ± 1.0
Hemoglobin (g/dl)	13.0 ± 1.5	13.9 ± 0.5
SaO_2 (%)	88.5 ± 4.0	99.4 ± 1.4

Figure 3 shows the typical aspect of a C6 glioma at the last stage of tumor growth for the three sizes of tumors. On BV and VSI images obtained from the nine large-size tumors, three regions could be distinguished: 1) a high BV region surrounding the tumor, which was found to correlate with a highly vascularized region where angiogenesis takes place; 2) a region where BV is very low, corresponding to necrosis; and 3) a region showing a similar or lower BV but a higher VSI than in the contralateral rat brain tissue, indicating the presence of larger vessels. This was confirmed by histology and was found to be associated with nonnecrotic tumor tissue. For the two medium-size tumors the central part of the tumors was characterized by a high blood volume instead of a low blood volume as for large-size tumors. This area was a mixture of necrotic and tumor tissue and showed numerous large vessels (10–80 μm in diameter). The four small-size tumors showed only two regions: a peripheral ring around the tumor with a high BV and the central region with a BV similar to that of the contralateral brain and a higher VSI, corresponding to nonnecrotic tumor tissue. We found edema in all tumors, mainly in the frontal cortex on the tumor side. In addition, pseudocysts could be observed in all but two rats.

Figure 4 shows the histogram of the vessel diameters in different regions of seven tumors used for the MRI/histology correlation. The distribution is centered around a radius of 3.1 μm and is narrow in the contralateral hemisphere (mean ± SD = 3.1 ± 1.3 μm and median = 3.1 μm), whereas the distribution is stretched towards higher diameters in tumoral regions (5.8 ± 4.1 μm and median 4.7 μm in the intratumoral region, 4.1 ± 2.1 μm and median 3.9 μm in the periphery of the tumor). This histogram is similar to fig. 6 in Dennie et al. (7), where the same tumor model was used.

MRI Quantitative Analysis

In Fig. 5, both BV and VSI, measured from the six rats with large tumors from Experiment 1, are plotted for three different regions: contralateral cortex, peritumoral, and intratumoral areas. BV is significantly lower ($P < 0.05$) in the tumor area (2.0 ± 0.7%) compared to the values in the contralateral cortex (4.3 ± 0.7%) and in the peritumoral area (4.0 ± 0.3%). No statistically significant difference

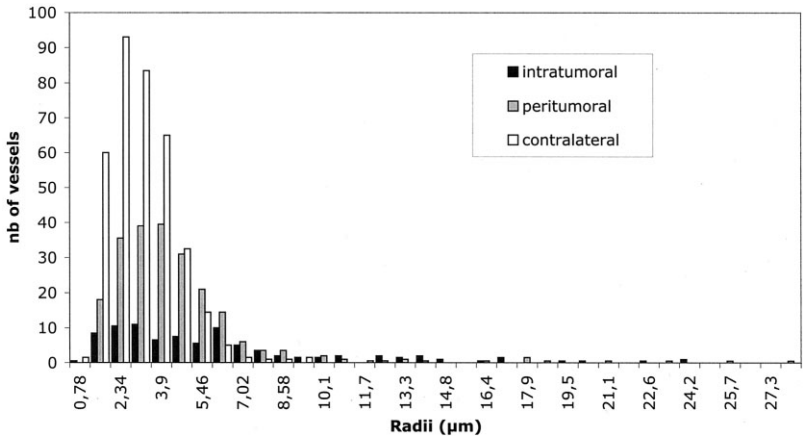

FIG. 4. Histogram of the mean vessel radii in seven rats for three different ROIs: periphery of the tumor, intratumoral area (viable tumor tissue), and contralateral cortex. Two histological slices were analyzed per animal and the mean vessel number per ROI is reported here. The microscope field of view was 0.27 mm^2 for each ROI. The total number of vessels counted on these ROIs was 1336.

between the contralateral cortex and peritumoral region was found. These values were calculated on pixels where the BV fraction was neither null nor higher than 17%. All VSIs in the three ROIs were significantly different from each other ($P < 0.05$), with intratumoral VSI_{MRI} (20.0 ± 6.3 µm) being much higher than peritumoral (7.5 ± 0.6 µm) and contralateral cortical (4.5 ± 0.8 µm) VSI_{MRI}.

Validation With Histologic Sections

VSI_{MRI} is plotted against VSI_{histo} in Fig. 6 for all ROIs of the seven rats which could be used for correlation between histology and MRI. A linear regression on all these points gives $VSI_{MRI} = 1.17 \times VSI_{histo}$ with $R^2 = 0.76$. The correlation coefficient measured by a Spearman rank correlation test is 0.74. Correlation is good especially for small values of VSI. Linear regression coefficients are, respectively, $R^2 = 0.83, 0.93, 0.97$ in the tumor, the peripheral area, and the contralateral cortex.

DISCUSSION

With an NMR sequence allowing simultaneous T_2 and T_2* assessment, we measured the BV and the VSI in three different regions of the tumor brain: in the contralateral cortex, in the periphery of the tumor, and within the tumor. We showed that intratumoral BV was significantly lower than contralateral BV and peritumoral BV and that VSI in tumor regions was significantly higher than VSI in the cortex, with VSI in the tumor higher than VSI in the periphery. The correlation between VSI_{MRI} and VSI_{histo} measurements was good.

BV Measurements

In large-size tumors, no significant difference was found between peritumoral BV (4.0 ± 0.3%) and contralateral cortical BV (4.3 ± 0.7%), although we observed a very important signal drop around the tumor on the postinjection T_2 and T_2* images. Two phenomena can explain this result: first, peritumoral BV was certainly underestimated, since high BV fraction pixels were excluded because of the upper limit of the method. Second, rats of Experiment 1 were under moderate hypoxia (PaO_2 = 70.5 mmHg), which increases BV by 15% in healthy brain areas (18), but does not significantly change BV in peritumoral zones for 15% of fractional inspired oxygen (19). We found a significantly smaller BV in the tumor (2.0 ± 0.7%) than in its periphery and in the contralateral area, in accordance with results on the same tumor model with injection of Sinerem (19). Julien-Dolbec et al. (19) have shown BV values

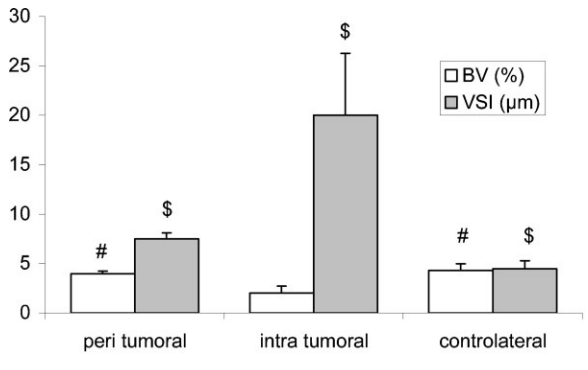

FIG. 5. VSI and BV MRI information: (n = 6 rats from the first experiment) $^{\#}P < 0.05$ with the nonparametric Wilcoxon test for the difference between peritumoral and intratumoral BV and for the difference between contralateral cortex and intratumoral BV. $^{\$}P < 0.05$ with the nonparametric Wilcoxon test for all VSI data.

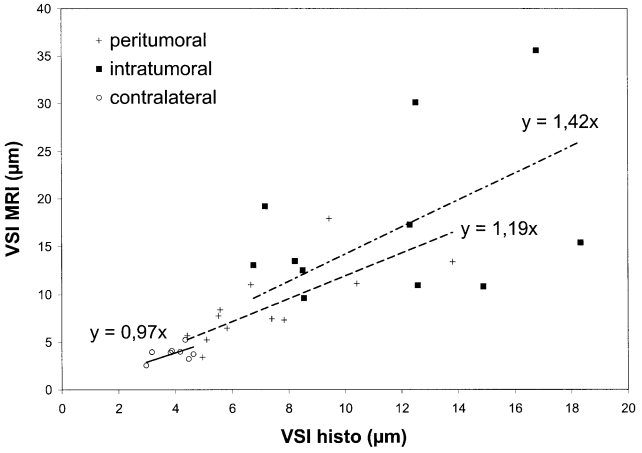

FIG. 6. Plot of VSI_{MRI} vs. VSI_{histo}. Spearman rank correlation test on all data yields $\rho_s = 0.74$.

smaller than ours, but in that study pixels where BV was null were taken into account for BV measurements and therefore decreased intratumoral BV values compared to our values. These results are in agreement with the vessel density qualitatively assessed as described in this article. It was clear on the corresponding histological slices that there was a higher vessel density at the margin of the tumor than in the nonnecrotic tumor tissue, a vessel density in the nonnecrotic tumor tissue similar to or lower than in the contralateral brain and no vessels in the large necrotic areas. These qualitative results are confirmed by two independent quantitative studies performed in the laboratory on the same experimental model at a similar growth stage (20,21). These results are also in agreement with histological data obtained by different authors on similar experimental brain tumor models (A15A5 tumor cells (1,22); GXII cells (23)). Luthert and Lantos (22) found that the vessel density decreased progressively from the periphery to the center of the tumor towards 20% that of the normal cortex, but the vessel size more than doubled. In addition, the surface area of the vessels reached a maximum at the tumor edge. Similar results were described by Zama et al. (23).

BV was high centrally in medium-size tumors and low centrally in nonnecrotic tissue in large tumors. One possible explanation which would be very attractive but has to be confirmed by additional experiments is that these three aspects represent the three different stages of tumor growth described by Holash et al. (24). First, there would be a co-optation of host vessels (small-size tumor with blood volume similar to the contralateral one), followed by vessels regression (medium-size tumor with an intermediate period where vessels are enlarged before regression), and finally, new vessel formation in the periphery of the tumor. Another explanation might be that these medium-size tumors (as well as the small-size tumors) are simply not normally growing tumors and that this might reflect an abnormal growing pattern, like degeneration.

VSI_{MRI} Measurements

The VSI value measured in a previous study (11) by MRI on the healthy rat brain was 4.8 μm in the cortex, similar to VSI_{MRI} measured here (4.5 ± 0.8 μm).

VSI_{MRI} in the tumor was more than twice VSI_{MRI} in the peritumoral zones (20.0 ± 6.3 μm vs. 7.5 ± 0.6 μm) and almost five times VSI_{MRI} obtained in the contralateral cortex. These results are in accordance with previous studies on the size of vessel diameters in tumors (1,7,25), which showed larger vessels in the tumor relative to the contralateral brain and also relative to the edge of the tumor (1).

In the present study, VSI_{MRI} was calculated using the same water diffusion coefficient for normal and tumor tissues. In Refs. 26–28, larger D values were measured in tumoral tissue than in healthy tissue. The diffusion coefficient in high-grade tumors can be twice the diffusion coefficient in normal gray matter, which would increase VSI_{MRI} in tumor tissue by a factor of $\sqrt{2}$. Using effective diffusion coefficients would therefore increase the difference between VSI_{MRI} in the tumoral and contralateral ROIs and reinforce the significance of the results obtained here, with increased VSI_{MRI} in the tumor. For more accurate VSI_{MRI} measurements, apparent diffusion coefficient measurements are recommended for forthcoming protocols.

The question of contrast agent leakage through the broken BBB should be evoked, since the last acquisition occurred about 60 min after the first injection. Dennie et al. (7) have shown that ΔR_2 and ΔR_2^*, following injection of a contrast agent (MION) similar to AMI-227, remained stable over 90 min in the tumor. Le Duc et al. (29) observed a lack of evolution during the first hour in the tumor after 200 μmol Fe/kg AMI-227 injection but measured a +12% ΔR_2 increase in the meantime in the peripheral rim of the tumor. VSI_{MRI} measurements in the intratumoral ROI should therefore not be affected by the leakage of the contrast agent through the broken BBB. Concerning the peripheral area, VSI_{MRI} is probably underestimated. Since ΔR_2 and ΔR_2^* are both linear with $\Delta\chi$ in the range 0.2–0.6 ppm (8,29), VSI_{MRI} is affected only by $(\Delta\chi)^{-1/2}$ (see Eq. 2). If we had injected 200 μmol Fe/kg 1 hr before imaging, VSI_{MRI} would have been underestimated by about–$(1.12)^{-1/2}$ or −6% according to the results of Le Duc et al. Since the total dose was fractionated (30 μmol Fe/kg, then 30 min later 100 μmol Fe/kg and again 30 min later, 100 μmol Fe/kg) and considering the measurement precision, the error introduced by the permeability of the BBB can thus be assumed to be negligible.

Dennie et al. (7) and Packard et al. (30) found a good correlation between $\Delta R_2^*/\Delta R_2$ and vessel size. However, this ratio is relative and Monte-Carlo simulations are necessary for histology correlation. Another study (10) proposed the use of an absolute parameter Q and found a good agreement between Q_{MRI} and Q_{histo} values estimated from Dennie et al. (7) experimental data. Applied to our experiments, Q can be calculated from the relationship:

$$Q = 0.4372\,\frac{(9D\cdot BV)^{1/3}}{(VSI)^{2/3}}.$$

Q equals 0.72 ±0.04 $s^{-1/3}$ in the peritumoral area, 0.31 ± 0.09 $s^{-1/3}$ in the tumor, and 1.04 ± 0.07 $s^{-1/3}$ in the contralateral side. This last value is higher than Q_{MRI} = 0.72 ± 0.21 $s^{-1/3}$ found in Jensen and Chandra (10), but our measurement was done in the contralateral cortex, whereas Dennie et al.'s measurement was performed in the striatum. From BV and VSI results obtained in our previous experiments on healthy rat brain (11), Q equals 0.92 $s^{-1/3}$ in the striatum, which is in accordance with Jensen and Chandra's computations. In the tumor, a good agreement is found (Q_{MRI} = 0.36 ± 0.15 $s^{-1/3}$).

Correlation Between VSI_{MRI} and VSI_{histo}

Each region is characterized by a distinct VSI_{MRI} value and this was verified by VSI computations from histograms published in the literature. From Weiss et al. (31) and Eq. 8 of our study, we obtained a VSI_{histo} of 3.4 μm in the normal brain. From fig. 6 in Dennie et al. (7), we calculated a VSI_{histo} of 3.8 μm in the gray matter and 9.4 μm in the tumor. These values in the contralateral side are in good agreement with our MRI mean value (4.5 ± 0.8 μm, Fig. 5), and Dennie et al.'s tumor value is comprised between our peripheral and intratumoral VSI_{MRI}. We have found a

proportionality coefficient of 1.17 between VSI_{MRI} and VSI_{histo} on all regions with higher MRI values in general. Looking tissue region by tissue region, very good correlation was obtained on the VSI measured in the contralateral hemisphere ($R^2 = 0.97$ and slope of 0.97), which validates MRI as a noninvasive tool for vessel size index assessments. In the tumor, the correlation is not as good ($R^2 = 0.83$ and slope of 1.42), probably because of the heterogeneity in the vessel density and in the vessel size in these regions (32,33). Note also that the histological technique we used detects all vessels (perfused and nonperfused), while MRI is sensitive only to perfused vessels (i.e., those accessible to the contrast agent). An improved interpretation of BV and VSI measurements might be obtained using a combination of histological techniques to allow not only the visualization of all vessels, as was done here, but also to distinguish those actually perfused (using, e.g., Hoechst as in Refs. 34,35).

CONCLUSION

In areas of necrosis, BV was null. In the viable tumor tissue, BV was lower than in the contralateral cortical area and VSI was much higher. In the periphery, BV was higher or equal to the contralateral cortical area and VSI was also higher. Necrosis, viable tumor tissue, and the periphery of the tumor can therefore be distinguished on the basis of BV and VSI measurements. The good correlation observed between VSI_{MRI} and VSI_{histo} demonstrates the potential of VSI imaging for in vivo tumor analysis and characterization.

VSI imaging is a powerful tool for assessing vessel size distribution and BV in cerebral tumors and for detecting small changes between the different regions. It would be interesting to apply this method at different stages of tumor growth to determine the correlation between VSI, BV, and tumor aggressiveness and to follow up the effect of antiangiogenic therapy. VSI analysis could then play a role in the diagnosis, therapeutic strategy, and follow-up.

ACKNOWLEDGMENTS

The authors thank Lucy Stride, ESRF France, for helpful corrections of the English of the manuscript and Dr. Canioni (Laboratoire de Résonance Magnétique des systèmes biologiques, Bordeaux, France) who kindly provided C6 cells.

REFERENCES

1. Deane BR, Lantos PL. The vasculature of experimental brain tumours. 1. A sequential light and electron microscope study of angiogenesis. J Neurol Sci 1981;49:55–66.
2. Delorme S, Knopp MV. Non-invasive vascular imaging: assessing tumour vascularity. Eur Radiol 1998;8:517–527.
3. Folkman J. Clinical applications of research on angiogenesis. N Engl J Med 1995;133:1757–1763.
4. Weidner N, Folkman J. Tumoral vascularity as a prognostic factor in cancer. Important Adv Oncol 1996;167–190.
5. Leon SP, Folkerth RD, Black PM. Microvessel density is a prognostic indicator for patients with astroglial brain tumors. Cancer 1996;77:362–372.
6. Okuhata Y, Brasch RC, Pham CD, Daldrup H, Wendland MF, Shames DM, Roberts TP. Tumor blood volume assays using contrast-enhanced magnetic resonance imaging: regional heterogeneity and postmortem artifacts. J Magn Reson Imag 1999;9:685–690.
7. Dennie J, Mandeville JB, Boxerman JL, Packard SD, Rosen BR, Weisskoff RM. NMR Imaging of changes in vascular morphology due to tumor angiogenesis. Magn Reson Med 1998;40:793–799.
8. Boxerman JL, Hamberg LM, Rosen B, Weisskoff RM. MR contrast due to intravascular magnetic susceptibility perturbations. Magn Reson Med 1995;34:555–566.
9. Donahue KM, Krouwer HG, Rand SD, Pathak AP, Marszalkowski CS, Censky SC, Prost RW. Utility of simultaneously acquired gradient-echo and spin-echo cerebral blood volume and morphology maps in brain tumor patients. Magn Reson Med 2000;43:845–853.
10. Jensen JH, Chandra R. MR imaging of microvasculature. Magn Reson Med 2000;44:224–230.
11. Troprès I, Grimault S, Vaeth A, Grillon E, Julien C, Payen JF, Lamalle L, Décorps M. Vessel size imaging. Magn Reson Med 2001;45:397–408.
12. Pathak AP, Donahue KM, Ward BD, Rebro KJ, Rand SD. Assessing tumor angiogenesis with dynamic susceptibility contrast fMRI: which morphologic correlates are relevant? In: Proc 9th Annual Meeting ISMRM, Glasgow, 2001. p 2243.
13. Yablonskiy DA, Haacke EM. Theory of NMR signal behavior in magnetically inhomogeneous tissues: the static dephasing regime. Magn Reson Med 1994;32:749–763.
14. Kiselev V, Posse S. Analytical model of susceptibility-Induced MR signal dephasing: effect of diffusion in a microvascular network. Magn Reson Med 1999;41:499–509.
15. Underwood EE. Stereology, or the quantitative evaluation of microstructures. J Microsc 1969;89:161–180.
16. Troprès I, Lamalle L, Farion R, Décorps M, Rémy C. Vessel size imaging at low contrast agent concentrations. 20th Annual Meeting European Society of Magnetic Resonance in Medicine and Biology, Rotterdam, 2003. p 249.
17. Hoehn-Berlage M. Diffusion-weighted NMR imaging: application to experimental focal cerebral ischemia. NMR Biomed 1995;8:345–358.
18. Julien-Dolbec C, Troprès I, Montigon O, Reutenauer H, Ziegler A, Décorps M, Payen JF. Regional response of cerebral blood volume to graded hypoxic hypoxia in rat brain. Br J Anaesth 2002;89:287–293.
19. Julien-Dolbec C, Troprès I, Montigon O, Farion R, Grillon E, Décorps M, Payen J-F, Rémy C. Functional properties of vessels in rat brain tumor: measurement of cerebral blood volume during graded hypoxic hypoxia. 19th Meeting European Society of Magnetic Resonance in Medicine and Biology, Cannes, France, 2002. p 92.
20. Péoc'h M, Le Duc G, Trayaud A, Farion R, Le Bas J-F, Pasquier B, Rémy C. Quantification and distribution of neovascularization following microinjection of C6 glioma cells in rat brain. Anticancer Res 1999;19:3025–3030.
21. Lamalle L, Troprès I, Péoc'h M, Farion R, Grillon E, Lahrech H, Usson Y, Décorps M, Rémy C. Blood volume and vessel size imaging: histological validation and vasculature characterization in rat brain during C6 glioma growth. In: ISMRM Workshop on "In vivo functional and molecular assessment of cancer," Santa Cruz, CA, 2002. p 24.
22. Luthert PJ, Lantos PL. A morphometric study of the microvasculature of a rat glioma. Neuropathol Appl Neurobiol 1985;11:461–473.
23. Zama A, Tamura M, Inoue HK. Three-dimensional observations on microvascular growth in rat glioma using a vascular casting method. J Cancer Res Clin Oncol 1991;117:396–402.
24. Holash J, Maisonpierre PC, Compton D, Boland P, Alexander CR, Zagzag D, Yancopoulos GD, Wiegand SJ. Vessel cooption, regression, and growth in tumors mediated by angiopoietins and VEGF. Science 1999;284:1994–1998.
25. Dewhirst MW, Tso CY, Oliver R, Gustafson CS, Secomb TW, Gross JF. Morphologic and hemodynamic comparison of tumor and healing normal tissue microvasculature. Int J Radiat Oncol Biol Phys 1989;17:91–99.
26. Eis M, Els T, Hoehn-Berlage M, Hossmann KA. Quantitative diffusion MR imaging of cerebral tumor and edema. Acta Neurochir Suppl (Wien) 1994;60:344–346.
27. Krabbe K, Gideon P, Wagn P, Hansen U, Thomsen C, Madsen F. MR diffusion imaging of human intracranial tumours. Neuroradiology 1997;39:483–489.
28. Wang Z, Su MY, Nalcioglu O. Measurement of tumor vascular volume and mean microvascular random flow velocity magnitude by dynamic Gd-DTPA-albumin enhanced and diffusion-weighted MRI. Magn Reson Med 1998;40:397–404.

29. Le Duc G, Péoc'h M, Rémy C, Charpy O, Muller RM, Le Bas J-F, Décorps M. Use of T2-weighted susceptibility contrast MRI for mapping the blood volume in the glioma-bearing rat brain. Magn Reson Med 1999; 42:754–761.
30. Packard SD, Niloff S, Terada K, Chiocca EA, Marota JJ, Rosen BR. Histological correlations of magnetic susceptibility contrast MR techniques. In: Proc 10th Annual Meeting ISMRM, Honolulu, 2002. p 197.
31. Weiss HR, Buchweitz E, Murtha TJ, Auletta M. Quantitative regional determination of morphometric indices of the total and perfused capillary network in the rat brain. Circ Res 1982;51:494–503.
32. Wesseling P, van der Laak JA, de Leeuw H, Ruiter DJ, Burger PC. Quantitative immunohistological analysis of the microvasculature in untreated human glioblastoma multiforme. Computer-assisted image analysis of whole-tumor sections. J Neurosurg 1994;81:902–909.
33. Fonchy E, Lahrech H, François-Joubert A, Dupeyre R, Benderbous S, Corot C, Farion R, Rubin C, Décorps M, Rémy C. A new gadolinium-based contrast agent for magnetic resonance imaging of brain tumors: kinetic study on a C6 rat glioma model. J Magn Reson Imag 2001;14: 97–105.
34. van der Sanden BP, Rozijn TH, Rijken PF, Peters HP, Heerschap A, van der Kogel AJ, Bovee WM. Noninvasive assessment of the functional neovasculature in 9L-glioma growing in rat brain by dynamic 1H magnetic resonance imaging of gadolinium uptake. J Cereb Blood Flow Metab 2000;20:861–870.
35. Zoula S, Rijken PF, Peters JP, Farion R, Van der Sanden BP, Van der Kogel AJ, Decorps M, Remy C. Pimonidazole binding in C6 rat brain glioma: relation with lipid droplet detection. Br J Cancer 2003;88: 1439–1444.
36. Underwood EE. Quantitative stereology. Reading, MA: Addison-Wesley; 1970.